

PAPER

Electron cyclotron power management for control of neoclassical tearing modes in the ITER baseline scenario

To cite this article: F.M. Poli *et al* 2018 *Nucl. Fusion* **58** 016007

View the [article online](#) for updates and enhancements.

Related content

- [On recent results in the modelling of neoclassical-tearing-mode stabilization via electron cyclotron current drive and their impact on the design of the upper EC launcher for ITER](#)
E. Poli, C. Angioni, F.J. Casson *et al.*
- [Chapter 3: MHD stability, operational limits and disruptions](#)
T.C. Hender, J.C. Wesley, J. Bialek *et al.*
- [Control of neoclassical tearing modes](#)
M. Maraschek

Recent citations

- [Survey of heating and current drive for K-DEMO](#)
D.R. Mikkelsen *et al*

Electron cyclotron power management for control of neoclassical tearing modes in the ITER baseline scenario

F.M. Poli¹ , E.D. Fredrickson¹, M.A. Henderson², S-H. Kim², N. Bertelli¹, E. Poli³, D. Farina⁴ and L. Figini⁴

¹ Princeton Plasma Physics Laboratory, Princeton, NJ 08543, United States of America

² ITER Organization, Route de Vinon-sur-Verdon, CS 90 046, 13067 St. Paul lez Durance Cedex, France

³ Max-Planck-Institute for Plasma Physics, 85748 Garching, Germany

⁴ Istituto di Fisica del Plasma, Consiglio Nazionale delle Ricerche (IFP CNR), Milano, Italy

E-mail: fpoli@pppl.gov

Received 29 March 2017, revised 27 August 2017

Accepted for publication 21 September 2017

Published 6 November 2017



CrossMark

Abstract

Time-dependent simulations are used to evolve plasma discharges in combination with a modified Rutherford equation for calculation of neoclassical tearing mode (NTM) stability in response to electron cyclotron (EC) feedback control in ITER. The main application of this integrated approach is to support the development of control algorithms by analyzing the plasma response with physics-based models and to assess how uncertainties in the detection of the magnetic island and in the EC alignment affect the ability of the ITER EC system to fulfill its purpose. Simulations indicate that it is critical to detect the island as soon as possible, before its size exceeds the EC deposition width, and that maintaining alignment with the rational surface within half of the EC deposition width is needed for stabilization and suppression of the modes, especially in the case of modes with helicity (2, 1). A broadening of the deposition profile, for example due to wave scattering by turbulence fluctuations or not well aligned beams, could even be favorable in the case of the (2, 1)-NTM, by relaxing an over-focussing of the EC beam and improving the stabilization at the mode onset. Pre-emptive control reduces the power needed for suppression and stabilization in the ITER baseline discharge to a maximum of 5 MW, which should be reserved and available to the upper launcher during the entire flat-top phase. Assuming continuous triggering of NTMs, with pre-emptive control ITER would be still able to demonstrate a fusion gain of $Q = 10$.

Keywords: NTM, electron cyclotron, ITER, control

(Some figures may appear in colour only in the online journal)

1. Introduction

Among the external heating and current drive systems planned in ITER, the electron cyclotron (EC) system has the highest flexibility. In fact, by combining the equatorial and the upper launcher, the EC can cover up to 85% of the plasma cross-section, missing about 10% of the edge and about 5%–10% near the axis, allowing for combined central heating, current profile tailoring and MHD stability control of sawteeth and neoclassical tearing modes (NTMs) [1–3].

Applications of the EC system include (a) breakdown and burn-thru assist in a limited plasma for flux consumption saving, (b) ramp-up assist and H-mode access (c) MHD control and central heating in the flat-top phase (d) ramp-down assist and exit from H-mode and (e) plasma termination. Every application has to be carefully balanced with the other heating and current drive sources for optimization of the heating and current drive (H&CD) resources.

An important application of the EC system is NTM control and stabilization, for which the upper launcher (UL) has been

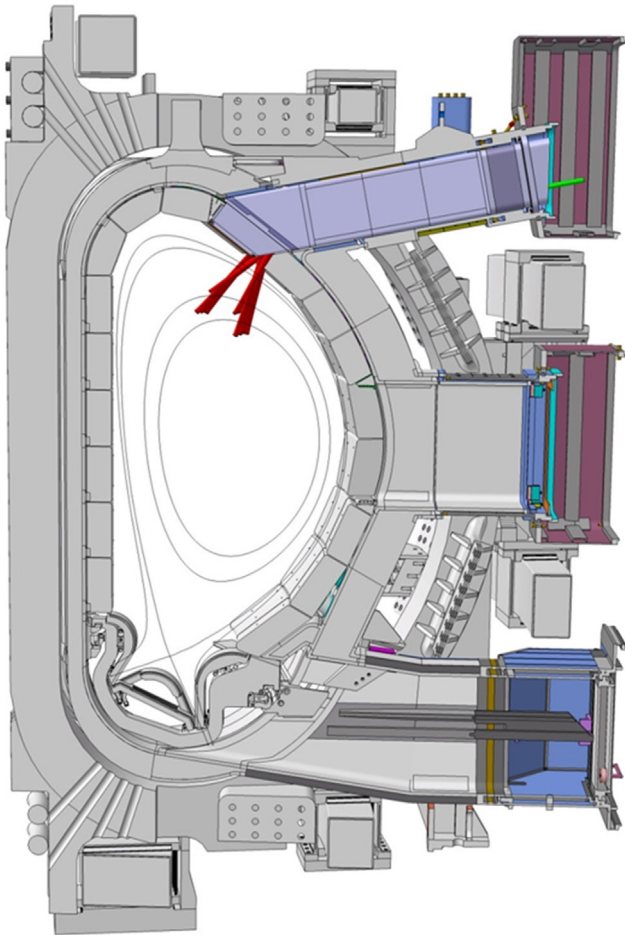


Figure 1. ITER plasma cross-section and structures, with the layout of the upper launcher and the beam aiming from the upper steering mirror (USM) and the lower steering mirror (LSM), aiming here respectively at the $q = 1.5$ and the $q = 2.0$ surface.

specifically designed, to provide localized deposition down to 2% of the minor radius [1–6]. The power is provided by 24 gyrotrons operating at a frequency of 170 GHz and power of 1 MW each, of which 0.83 MW are delivered to the plasma on account of transmission losses from the gyrotron diamond window to the plasma boundary. Figure 1 shows the layout of the UL, which is comprised of four ports, each housing eight beam lines, arrayed in an upper and lower row of four waveguides each, dubbed upper steering (USM) and lower steering (LSM) mirror. The UL can deliver the total 20 MW of power, with up to two thirds on either steering mirror.

Localized current drive by radiofrequency waves, deposited inside a magnetic island, is an effective way of stabilizing nonlinear tearing modes, as shown in the pioneering work by Reiman, which explores the case of lower hybrid waves [7]. The most successful experimental application of rf waves for tearing mode stabilization has however been demonstrated with injection of EC waves, which can provide the necessary profile localization at the rational surfaces $q = 1.5$ and $q = 2$ (see, for example, the review by Maraschek [8]).

Assessments of the power needed for NTM control and stabilization in the ITER baseline are usually expressed in terms of the figure of merit $\eta_{\text{NTM}} \equiv j_{\text{CD}}/j_{\text{BS}}$, defined as the

ratio of the EC current density to the bootstrap current density at the rational surface. Criteria for the value of η_{NTM} go back to the work by Hegna and Callen [9], who predicted for ITER $\eta_{\text{NTM}} = 1.5$, followed by Zohm [6] who predicted $\eta_{\text{NTM}} = 1.2$. The derivation of η_{NTM} has since been the subject of progressively more accurate derivations, which are surveyed in the review by Poli [10]. However, those offline calculations did not account for modifications of the magnetic equilibrium and of the pressure profiles in response to the EC heating and current drive as they evolve during the plasma discharge.

Herein we describe a different approach, more consistent, but not yet entirely self-consistent, where a modified Rutherford equation (MRE) is solved during the simulation and a feedback control is used to steer the mirrors and to change the EC power level in response to the NTM stability. The main application of this integrated approach is to support the development of control algorithms and to assess the effect of uncertainties in the detection of the magnetic island and in the alignment of the EC with the resonant surface on the ability of the ITER EC system to fulfill its design requirements. A second, important application is scenario development and design of discharges that satisfy at the same time stability and performance, since one of the ITER goals is to demonstrate operation at fusion gain of $Q = 10$, where $Q = 5P_{\alpha}/P_{\text{ext}}$ is the ratio of the fusion power from self-heating alpha power P_{α} to the power from external sources P_{ext} .

The approach undertaken for the calculations in TRANSP [11] is described in section 2 and the MRE adopted here is summarized in the appendix. Section 3 discusses the stability in the ITER baseline plasma, by comparing two simulations that differ only by 6% in the pedestal pressure, but significantly in the plasma performance and in the NTM stability. Section 4.1 discusses the control and stabilization of modes that have grown above the critical size, section 4.2 discusses pre-emptive control and sections 5 and 6 and how this is affected by the alignment between the EC deposition and the rational surfaces and by a broadening of the deposition profile. Finally, section 7 concludes with some remarks on the implications of these results on discharge design for performance and control, on the required accuracy in the EC alignment, as well as giving recommendations for further analysis and for research on control algorithms applied to ITER.

2. Calculation of NTM stability in TRANSP, with simulated EC feedback control

In order to assess the EC control system requirements, it is important to simulate the evolution of the NTM island in combination with the plasma magnetic equilibrium and the kinetic profiles, as they evolve in response to the external heating and current drive. Approaches based on a modified form of the Rutherford equation [12] are routinely used for calculation of NTM stability, as well as reduced models for real-time control oriented algorithms [13].

The TRANSP equilibrium and transport solver [11] has a unique capability of being used in conjunction with so-called ‘expert files’. Expert files are external coding that are linked

to the main executable and that allow users to manipulate the simulations by including additional features. A direct application of expert files is for simulations dedicated to develop control algorithms and it has been applied on NSTX-U for control of the plasma performance [14, 15] and of plasma rotation [16] with neutral beam injection. In this respect expert files can provide valuable inputs for control requirements, diagnostic sensitivity or development of actuator power sharing control algorithms, because they allow the study of the plasma response to external perturbations in the presence of high-fidelity physics models.

In order to provide a simulated response of the plasma, a MRE has been interfaced with TRANSP. The MRE used here is based on the approach by Fredrickson [17], which was validated against (3,2)-NTMs on TFTR [18]. This approach uses the so-called Δ' formalism to deal with the boundary layer physics inherent in tearing mode theory [19]. It has been shown that a full solution of the resistive magneto-hydrodynamic (MHD) equations is not necessary to determine the stability of a given current profile to tearing modes. In this approach the perturbed helical flux function $\psi_{m,n}$ is found through integration of the second order partial differential equation:

$$\left[\frac{\partial^2}{\partial r^2} + \frac{1}{r} \frac{\partial}{\partial r} - \frac{m^2}{r^2} - \left(\frac{\partial J_0}{\partial \psi_0} \right) \right] \psi_{m,n} = 0 \quad (1)$$

in the region between the plasma magnetic axis and the rational surface (the boundary layer) and in the region from the rational surface to the plasma boundary, subject to the constraint that $\psi_{m,n}$ matches across the rational surface. For the cylindrical case, $\partial J_0 / \partial \psi_0$ is just a function of $q_0(r)$. The code interfaced in TRANSP solves a quasi-cylindrical version of this equation by using both the unperturbed current density $J_0(r)$ and safety factor $q_0(r)$ profiles from TRANSP. As TRANSP separately calculates the ECCD current, this term could be calculated excluding the contribution of the equilibrium ECCD perturbation to the total current, thus avoiding potential double counting [20]. The normalized discontinuity in the derivative at the resonant surface r_s :

$$\Delta'_{m,n} = \frac{\frac{\partial \psi_{m,n}^-}{\partial r} - \frac{\partial \psi_{m,n}^+}{\partial r}}{\psi_{m,n}} \Bigg|_{r=r_s} \quad (2)$$

represents the drive or damping for the island. For finite size islands, $\Delta'_{m,n}(w)$ is calculated by taking the discontinuity between the inner and outer island edges, with the perturbed flux, $\psi_{m,n}$ assumed constant across the island [17, 18, 21, 22]. As tearing modes are generally not predicted to be linearly unstable (with the possible exception of the (2,1)), a 'seed island' that might originate from ELMs or sawtooth crashes is needed to trigger island growth. The island evolution is calculated assuming a fixed minimum island size, $w_{\min} \approx 10^{-3}a$, where a is the plasma minor radius⁵. The island will only grow unstable when the stabilizing effects due to curvature and

⁵ The plasma minor radius is defined in TRANSP as the average radius, calculated at midplane from the outer and inner plasma boundary $0.5(R_{\text{ou}} - R_{\text{in}})$.

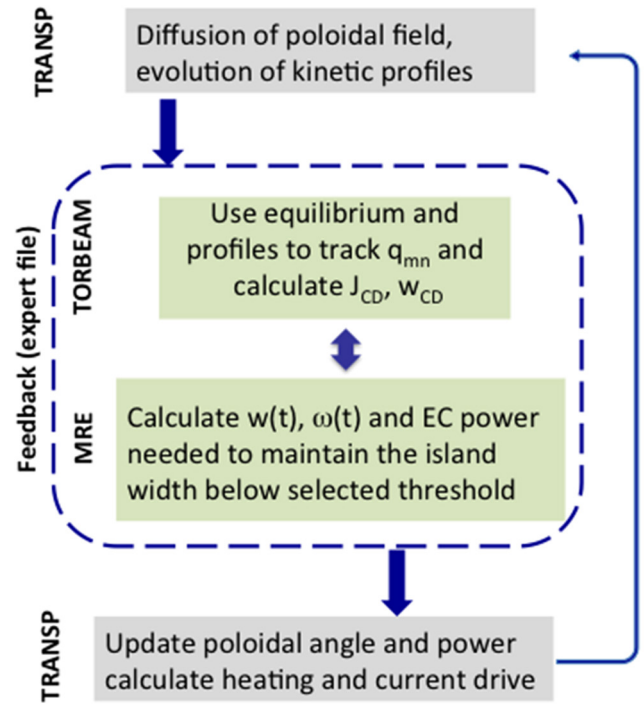


Figure 2. Schematics of the interface between TRANSP and the EC controller for NTM stabilization.

polarization current, which dominate at small-island size, are dominated by the destabilizing contribution of the neoclassical drive and the total $\Delta'_{\text{tot}}(w)$ becomes positive. This could be modified in the future by only making this seed island finite during ELMs or at sawtooth crashes, for example.

The contributions from the EC heating and current drive have been added to the original MRE using the formulation by Bertelli *et al* [23] and De Lazzari *et al* [24]. Details of the terms added to the MRE for the evolution of the island width are summarized in the appendix and a schematic of the interface and of the EC feedback control is shown in figure 2.

The feedback control consists of two parts: one provides the evolution of the width and rotation frequency of the island and the other interfaces the calculation of the island stability with a feedback control on the poloidal steering mechanism and of the input power. The part that deals with the control of the EC power and steering uses the beam tracing code TORBEAM [25] and can be pre-programmed for combined applications, like sawtooth and NTM tracking and control. There are three different time steps in TRANSP, those associated with the evolution of the magnetic equilibrium and of the transport are adjusted by the respective solvers in order to satisfy convergence of the solution, while the time step of the heating and current drive sources is pre-selected by the user. The interface between TRANSP and the MRE-based feedback control is implemented through an expert file. The calculations in the expert file are done on the time step δt_{HCD} of the heating and current drive sources, which is selected here according to the constraints imposed by the hardware. The longest time scale considered is 3 s and is a mechanical limit imposed by the switching mechanism of the EC transmission path between launchers. Other time scales of the hardware to

be considered include (a) the time needed to turn-on and off a gyrotron, which is of the order of tens of milliseconds (b) the UL steering mechanism can scan the entire poloidal angle range of 30 degrees in about 2 s, with steps of 0.02 degrees, therefore continuous mirror steering for tracking the island requires an additional several milliseconds (c) the computation of real-time feedback control algorithm would be fast and of the order of a few milliseconds. These additional sources of delay are assumed not to impose any significant additional latency over the time-scale of switching the EC transmission path between EC launchers.

In the absence of any feedback control the simulation would update the H&CD sources according to preset waveforms at time t_1 and evolve the magnetic equilibrium and transport between t_1 and $t_2 = t_1 + \delta t_{\text{HCD}}$ for fixed H&CD source parameters. When the interface shown in figure 2 is used, at t_1 TORBEAM uses the magnetic equilibrium and pressure profiles to calculate the ray trajectories and the current drive profiles and to align the system with the $q = 2$ and the $q = 1.5$ surfaces if alignment is lost. The MRE evolves the magnetic island width and rotation frequency between t_1 and t_2 with internal time steps of 25ms, under a given input power at t_1 , poloidal steering angle and calculated EC current density profile.

There are several limitations to this approach. The MRE is evolved at this time within an external interface, thus the evolution of the island is calculated using the magnetic equilibrium and kinetic profiles at time t_1 , while the magnetic equilibrium and kinetic profiles are evolved in TRANSP over shorter time scales. If the control interface decides to update the input power in order to suppress the island, then the new value is given to TRANSP, which will update and use the new power and current for the equilibrium and temperature profile evolution. This is consistent with what would be done during feedback control experiments, where ray-tracing calculations would be performed based on real-time reconstruction of the magnetic equilibrium and of the density and temperature profiles at a given time and where there is a latency between the time the new EC parameters are communicated to the plasma control system and the time the power and steering angle are actually updated. However, the plasma would evolve over MHD time scales under the presence of the magnetic island and this is not described accurately in the interface yet. More consistent calculations should evolve the island over the faster time scales of transport, as well as include the effect of a finite island width on the temperature (and density) profiles, for example by increasing artificially the conductivity (and diffusivity) profile locally to reduce the neoclassical drive. Also, in TRANSP both the steering angle and the input power are updated during the same time scale δt_{HCD} , while the time required to turn-on/off a gyrotron and to make small adjustments to the poloidal angle are much shorter than the time required to switch between transmission lines. In practice, all simulations described here have an uncertainty on the results that is equal to the time step used for the update of the EC parameters, δt_{HCD} .

While some of these effects, like the evolution of the magnetic island over transport time scales, the inclusion of toroidal

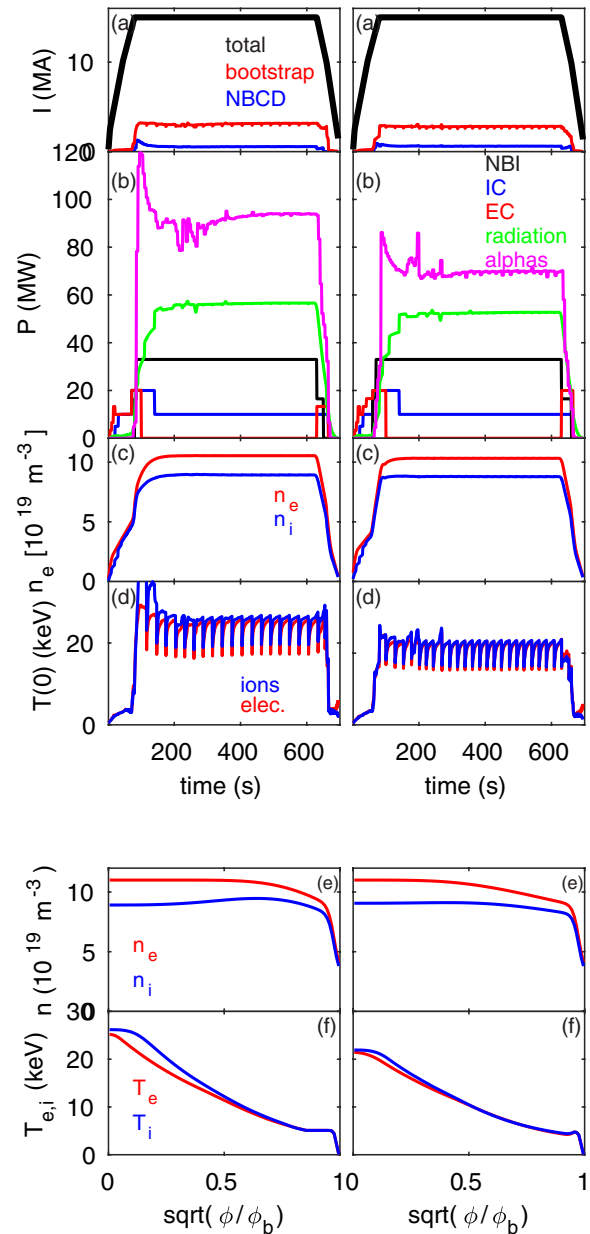


Figure 3. Time traces for the baseline scenario for two assumptions of the L-H transition time: at the end of the ramp-up phase (left) and at about three quarters of the ramp-up phase (right column). (a) plasma current, NB driven current and bootstrap current (b) injected external power, radiated power and α power. (c) line integrated density for electrons, ions and impurities, (d) electron and ion temperature, central value. (e) density profiles at 480 s (f) temperature profiles at 480 s.

effects in the calculation of the tearing stability term, and corrections in the calculation of $\Delta'(w)$ to avoid counting the EC current twice [20], will be accounted for in future work, we note here that a self-consistent approach would be possible only within the context of 3D MHD simulations [26].

Only cases with continuous EC injection for NTM control are discussed in this paper. In fact, the EC power modulation to synchronize the injection window with the island O-point is important only when the EC deposition width is larger than the magnetic island size [10, 23, 27], a situation that is not observed in the simulations discussed here.

3. NTM stability in the baseline scenario

Figure 3 shows two TRANSP simulations of the ITER 15 MA ELMy H-mode, used as a reference in this work for the NTM analysis. The current ramp-up phase is 80s long, with the plasma being diverted at about 12s and the radio-frequency heating and current drive being turned-on shortly after. The electron density is built-up fast to $2 \times 10^{19} \text{ m}^{-3}$ within the first 20s to provide a background plasma for good absorption of both Electron and ion cyclotron waves. The EC power is turned-off in the flattop in both simulations, to provide a reference case for the NTM stability with EC control discussed in the following sections. The time step used here is therefore not subject to NTM feedback constraints and is chosen equal to 5s. For comparison, the energy confinement time in these simulations is 3–4s. The electron density profile is prescribed in time, while the electron and ion temperature profiles are evolved using the GLF23 [28, 29] turbulence transport model. The sawtooth cycle is predicted using the Porcelli mixing method [30] and all sawtooth crashes are triggered because fast ion effects are insufficient to stabilize the internal kink mode (condition expressed by equation (13) in [30]). The pedestal width and height are interpolated from a lookup table constructed with the EPED1 peeling-ballooning stability model [31]. EPED1 uses input parameters such as pedestal density, shape parameters, the plasma composition Z_{eff} and the normalized magnetic to plasma pressure β_N [32] to predict the pedestal width and height. There are 987 EPED1 calculations in the look-up table covering the range of parameters expected for the ITER baseline scenario. Because the pedestal width and height are interpolated at each time step, the discharge evolution and the core profile evolution respond nonlinearly to variations in β_N , shape and Z_{eff} , causing the variation in amplitude in the calculated P_α trace. The impurity profile shapes are the same as the electron density profile, rescaled according to a fraction that is prescribed in time; impurity fraction levels assumed here in the flattop phase are Berillium at 2% of the electron density, Argon 0.1% and Tungsten up to 10^{-5} of the electron density. The dominant contribution to the radiation is from Bremsstrahlung and from Tungsten line radiation. However, because the impurity profiles are not calculated self-consistently, there are large uncertainties on the calculated radiation power. The profile of Z_{eff} is fairly broad with a value of 1.8 on axis, and $Z_{\text{eff}}(q = 1.5) = 1.68$ and $Z_{\text{eff}}(q = 2.0) = 1.65$ at the two resonant surfaces of interest. Because of these assumptions, and because the electron density is prescribed, the difference in the interpolated T_{ped} is small.

The two simulations differ in the time of entry into H-mode, which is 80s in the case shown in the left column and 65s in the case shown in the right column. They also have a different pedestal pressure gradient, under the assumption that ITER will operate with ELM mitigation and suppression techniques and that the pedestal pressure gradient would be lower than the upper limit predicted by EPED1. The transition from L- to H-mode is set by increasing the level of injected power above the threshold power provided by the ITPA scaling [33] and by

changing the density profile from a more peaked to a more flat profile with a pedestal. After the L–H transition the electron density rapidly builds-up to the flattop value of $0.85n_G$. Since entry to H-mode is imposed in both cases at half the Greenwald density n_G , the two cases are also using different density evolution during the last third of the current ramp-up phase.

The large increase in the alpha power at the entry to burn is a consequence of using a prescribed density profile across the L–H transition and it is related to a similar transient increase in the pedestal temperature to satisfy the pedestal pressure calculated from the EPED1 lookup table. Self-consistent simulations should evolve all transport channels with a coupled core-edge plasma model, for an assessment of the conditions of entry to H-mode in response to the heating and current drive sources mix. Since the density profile is prescribed, the two selected cases are meant to show how uncertainties in the underlying assumptions can affect the conclusions on NTM stability and EC power assessment. With small differences in the density pedestal structure and in the L–H transition assumptions, the two simulations evolve to different states. The plasma with earlier H-mode access has a core temperature that is about 20% lower (6% lower pedestal temperature) in the flattop phase, which results in a drop of P_α of about 30%.

Figure 4 compares the evolution of the bootstrap current at the resonant surfaces where $q = 1.5$ and $q = 2.0$. The lower pedestal pressure gradient results in a lower bootstrap current at the $q = 2$ surface and therefore in a lower amplitude of the neoclassical contribution to the (2, 1)-NTM. Since the density profiles are flat and the temperature profiles are rather stiff in the core, differences in the bootstrap current at the $q = 1.5$ surface are smaller. The two simulations have thus different neoclassical drive, which results in differences in the island width of about 20% at the $q = 1.5$ surface and about 50% at the $q = 2.0$ surface in the flattop phase. While earlier L–H transition results in an earlier appearance of the (2, 1)-NTM, the growth of both modes is slower, mostly due to the less steep rise of the bootstrap current at the respective rational surfaces. The MRE is solved for island width normalized to the plasma minor radius. For graphical purposes and ease of reading these distances are converted to physical quantities using the average plasma minor radius, $a = 201 \text{ cm}$.

3.1. Evolution of the NTMs in the baseline simulation

Figure 5 (top panel) shows the dominant contributions to the island width growth for the two plasma simulations in the flattop phase at 480s, as calculated by the MRE. The calculations are done for the $(m, n) = (3, 2)$ and $(2, 1)$ modes, in the absence of EC heating and current drive. Shown in the figure are the classical term $\Delta'_{m,n}(w)$ (blue), the contribution from the polarization current $\Delta'_{\text{pol}}(w)$ (magenta, equation (A.4)) which introduces a stabilization effect at small island width, the neoclassical contribution $\Delta'_{\text{NC}}(w)$ (red shaded area, equation (A.2)) and the total growth rate $\Delta'_{\text{tot}}(w)$ (black shaded area). The magnetic geometry contribution

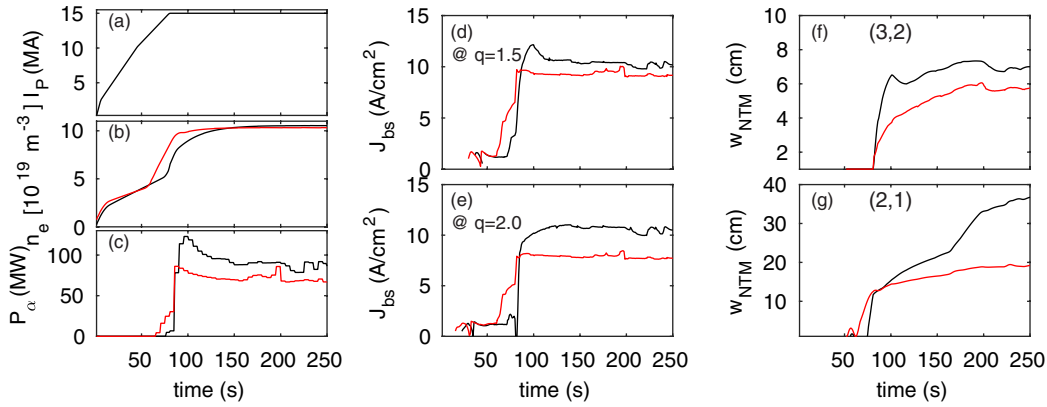


Figure 4. NTM stability for two different assumptions on the density evolution and the entry to H-mode. The red line refers to the early H-mode case, the black line to the late H-mode case. Note that no control with EC is applied in these simulations. Left panel: (a) plasma current ramp-up (b) line averaged density (c) alpha particle self-heating power. Central panel: bootstrap current density for the same cases, calculated at (d) $q = 1.5$ and at (e) $q = 2.0$. Right panel: width of the NTM island calculated for the (f) (3,2) mode and for the (g) (2,1) mode.

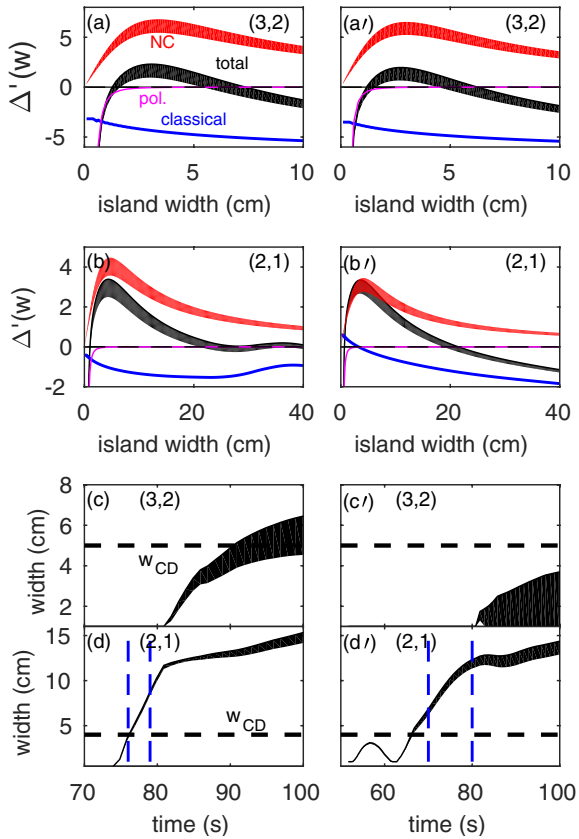


Figure 5. Left: case of large pedestal pressure. Right: case of low pedestal pressure. Top: Δ' terms for the (3,2) and the (2,1) modes, calculated at 480 s; neoclassical contribution $\Delta'_{\text{NC}}(w)$ (red), classical tearing term (blue), small-island stabilization contribution from the polarization term $\Delta'_{\text{pol}}(w)$ (magenta) and total contribution $\Delta'_{\text{tot}}(w)$ (black). The $\Delta'_{\text{NC}}(w)$ term accounts for uncertainties in the value of k_1 , which are reflected in the total growth rate. Bottom: time evolution of the width of the NTM island at $q = 1.5$ and $q = 2.0$; the colored area accounts for the variation due to the choice of k_1 . The average flattop value of the ECCD deposition with w_{CD} is shown for comparison. Vertical lines indicate the time window where the (2,1)-NTM is expected to lock.

$\Delta'_{\text{GGJ}}(w)$ term (equation (A.5)) also introduces a stabilization for small island width and is included in the calculations, but not shown in figure 5, being negligible compared to the others. The shaded area indicates the range of uncertainty in the results for two choices of the constant k_1 in the neoclassical contribution (see equation (A.2)), namely $k_1 = 0.20$ and $k_1 = 0.16$, which correspond respectively to the values of 3.2 and 2.6 used by Sauter [34] and derived in the case of large aspect ratio tokamaks [35, 36] and geometrical effects [37]. The coefficient in the contribution from the polarization current is instead maintained at unity. Increasing this coefficient according to previous estimates for ITER [34] increases the seed island size by about 25%. However, this does not affect the main conclusions on our analysis on the levels of power needed, especially in the case of the (2,1)-NTM, which is predicted to grow to a width comparable to the EC deposition width and lock within a few seconds.

There are two solutions for $\Delta'_{\text{tot}}(w) = 0$, one at small width, which corresponds to the onset of the mode, and one at large width, dubbed w_{sat} (saturated island) which corresponds to the stabilization of the magnetic island from the equilibrium current. The onset of the NTM depends on the balance between the destabilizing contribution and the stabilizing effects at small island width.

The (3,2)-NTM and the (2,1) are predicted to grow unstable when their width exceeds about 1.0–1.5 cm, which is smaller than the estimated ideal resolution of the ECE diagnostic, which is about 2 cm [38]. Although the accuracy of the magnetic equilibrium reconstruction by the PCS requirement [39] should be sufficient to provide the location of the resonant surfaces within 2 cm, in this work this limit has been conservatively increased to 3 cm reflecting the projection from the reconstruction methods used on present devices, such as JT-60U and DIII-D [40]. The width corresponding to the maximum growth rate Δ'_{max} is $w_{\text{max}} \simeq 4$ cm for both modes. The value of w_{max} is the reference target for NTM stabilization and for the calculations of η_{NTM} from the condition $dw/dt = 0$

[10, 23]. Techniques for NTM control should aim at dropping the value of Δ'_{\max} to zero and maintaining the size of the island below w_{\max} [40].

The value of w_{sat} is about 5–7 cm in the case of the (3, 2) for both plasma simulations, while it varies between 20 and 40 cm for the (2, 1)-NTM depending on k_1 and on the pressure pedestal height. The pressure profile flattening inside the island leads to a relative degradation of the confinement τ_E , which can be estimated using the *belt* model [41]:

$$\frac{\Delta\tau_E}{\tau_E} = -4\rho_s^3 \frac{w_{\text{sat}}}{a} \quad (3)$$

where ρ_s is the value of normalized minor radius where the NTM appears. The confinement degradation would be around 4% in the case of a (3, 2)-NTM at $\rho_s \simeq 0.65$ and with $w_{\text{sat}} \simeq 7$ cm and about 7% for an (2, 1)-NTM at $\rho_s \simeq 0.80$ of comparable size, having assumed here that the (2, 1)-NTM would lock well before saturating and that the control feedback is preventing the island from growing above 6–7 cm. It should be noted that w_{sat} for the (2, 1)-NTM is sensitive to details of the pressure profiles and—in particular—to the pedestal pressure gradient. Differences in the values obtained here and those previously reported [27] are to be attributed mostly to the different pressure profiles and plasma current profiles used.

The features at large island width (see figure 5(b)) are an effect of calculating the tearing stability term from an integration of the current profile over the tearing layer rather than using a reduced, parametrized model [17–19].

When the island width achieves large values, hitting the location of the pedestal, the large amplitude in the bootstrap current causes the $\Delta'_{m,n}(w)$ term to deviate from monotonic. This change in slope of the classical term is not observed in the plasma discharge simulation with lower pedestal pressure.

Figures 5(c)–(d) show the evolution of the islands at $q = 1.5$ and $q = 2$ at the first time the NTM appears, soon after entry to H-mode. The entry to H-mode is perhaps the most challenging phase for NTM control: depending on the density build-up rate compared to the plasma current ramp rate and how the heating and current drive sources are used to access H-mode, the poloidal flux surfaces might not have reached a stationary state, challenging the tracking of the rational surfaces where NTMs are most likely to be triggered. In addition, if the (2, 1)-NTM is not controlled soon after its appearance, there is risk for a drop in the stored energy and a L-mode back transition. In this event, there could be a critical configuration in which the EC has to prevent NTM generation to maintain the H-mode.

The average value of the deposition width of the ECCD, w_{CD} , in the current flattop phase is shown for comparison. The latter is calculated as the full width at half maximum of the EC current density profile, which is assumed to be a perfectly focussed beam, gaussian profile. The stabilization at the $q = 2$ surface is challenged by the fast growth of the mode to a width comparable to the EC deposition w_{CD} , which is less than two seconds in the case with higher pedestal pressure and about fifteen seconds in the plasma with lower pedestal pressure. In both cases the rotation frequency of the (2, 1)-NTM is predicted to increase to about 200 Hz after triggering, and the

island to lock over time scales of 5–10 s, i.e. before the island width has reached 10 cm. This is consistent with previous estimates that the (2, 1)-NTM would lock on ITER at a width of about 8 cm [42, 43].

The uncertainty in the width of the (3, 2)-NTM is large and simulations predict this mode to change between stable or unstable depending on the assumptions on the density profile evolution, the assumption on the calibrating coefficient k_1 and the pedestal pressure gradient. Because of the combination of a small seed island, narrow deposition width and fast growth rate, early detection is a critical requirement for the success of NTM control on ITER, especially in the case of the (2, 1)-NTM. Assuming that the threshold for the detection of the island is 2–4 cm accounting for degradation of signal to noise ratio and that the requested power for stabilization is made available to the upper launcher within the 3 s of the switch mechanism, the island would have reached about 7–8 cm and eventually locked by the time the EC power is available on the $q = 2$ surface. This is the case for both assumptions on the ramp-up evolution. It is therefore critical that stabilization of this mode is achieved within a few seconds from its trigger, since there might be not sufficient time between the detection of this island and its locking. For this reason, the discussion in the remainder of this paper focusses on finding conditions that prevent the island from growing above a few centimeters, typically 6–7 cm.

4. NTM control and stabilization

Approaches to NTM control can be divided into two categories: control of modes that have grown above the threshold for detection and prevention of the development of instabilities. The techniques most widely used in present-day tokamaks and the main results until 2012 are reviewed by Maraschek [8]. Subsequent to the publication of this review, progress has been made in the search and suppression of NTMs and in pre-emptive control on DIII-D [44–46], TCV [47–50] and ASDEX-U [51, 52]. This section describes simulations where the input power is adjusted in response to the measured NTM width and growth rate (section 4.1) and where a constant amount of power is instead maintained on each rational surface for pre-emptive control (section 4.2). It is shown that the requested power is significantly lower in the case of pre-emptive control, provided the alignment of the EC deposition with the rational surface is maintained within $0.5w_{\text{CD}}$.

4.1. Stabilization and suppression of an evolved island

This section discusses simulations with feedback control, where the EC input power is changed in response to the NTM width in order to either suppress the NTM or to reduce its width to a size that corresponds to the threshold for detection, w_{ECE} . The time step used here for the EC calculations is $\delta t_{\text{HCD}} = 3$ s, which corresponds to the upper limit imposed by the switch that redirects the power from one mirror to another. For example, if the EC power is directed to the equatorial launcher for core heating and current profile tailoring and an

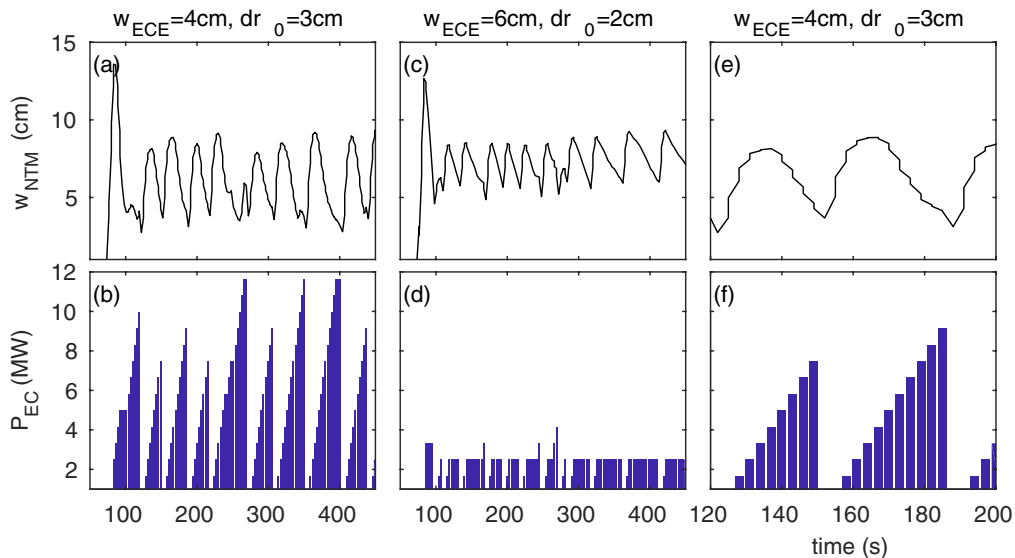


Figure 6. Results from TRANSP/MRE simulations of the (2,1)-NTM in the plasma with higher pedestal pressure gradient, where the EC input power is changed in response to the island width and growth rate, for the plasma simulation with higher pedestal pressure. For each case the NTM island width and the input EC power are shown. (a)–(b) case of tolerance on misalignment of 3 cm and threshold for detection of 4 cm (c)–(d) case of tolerance for misalignment of 2 cm and threshold for detection of 6 cm (e)–(f) expanded view of the case shown in the first column.

NTM is detected on either the $q = 1.5$ or the $q = 2$ surface, then three seconds are needed for the power to be available on the upper launcher. The time step used in the simulations mimics such delay in the response of the system, so that the EC power is updated in TRANSP only every 3 s.

We interpret here the calculated width and $\Delta'_{\text{tot}}(w)$ as proxies for the detection of the NTM from the ECE diagnostics and from the magnetic measurements. The feedback control procedure is programmed as follows: (a) the EC power is turned on only when the island width grows above w_{ECE} (b) if the island width has shrunk below w_{ECE} and $\Delta'_{\text{tot}}(w) \leq 0$ the input power is dropped to zero, this case corresponding to a fully suppressed island (c) if $\Delta'_{\text{tot}}(w) > 0$ and $w > w_{\text{ECE}}$ the MRE calculates how much power is needed to reduce $\Delta'_{\text{tot}}(w)$ to zero and feeds back this power level to TRANSP (d) if $\Delta'_{\text{tot}}(w) > 0$ and $w < w_{\text{ECE}}$ the EC input power is maintained constant.

Figure 6 shows the results for the plasma with higher pedestal pressure for two assumptions. In one case the detection threshold is $w_{\text{ECE}} = 4$ cm and the requested tolerance on the alignment of the EC with the resonant surface is $dr_0 = 3$ cm. In the other case the detection threshold is $w_{\text{ECE}} = 6$ cm and the requested tolerance is $dr_0 = 2$ cm.

An upper limit of 13.4 MW is set on the power that can be delivered to the LSM, which is tracking the $q = 2$ surface. Consequently, the upper limit on the power that can be delivered to the USM, which is tracking the $q = 1.5$ surface, is 6.67 MW.

In both cases, the island grows to a maximum size of about 8–10 cm; however, in the case with better alignment, the investment of power is lower, which does not really matter since in both cases the island width would be too large to avoid locking.

Since the kinetic profiles and the magnetic equilibrium evolve during these 3 s and since, as explained in section 2, the evolution of the magnetic island is calculated assuming frozen

equilibrium and pressure profiles during these 3 s, there is an uncertainty on the power that is calculated under frozen conditions. As shown in the expanded view of figures 6(e)–(f), the uncertainty on these results is of about one gyrotron each time the HCD sources are calculated.

It is noted that the NTM promptly grows back shortly after the EC power has been removed from the resonant surface. This is a consequence of the large neoclassical drive and of the lack of a validated reduced model for the calculation of the threshold for NTM triggering. In practice, it is like these simulations are assuming a ‘sea’ of islands with width just below the critical size for onset, NTMs are ready to be triggered at the appearance of any perturbation. It has been observed that the large β on ITER would make NTM metastable and susceptible of being triggered not only from sawtooth crashes, as observed in present-day experiments, but also from other external or internal disturbances, like ELMs and pellets [34], or possibly electromagnetic turbulence [53–56]. However, the MRE is intrinsically a reduced model and the threshold effects on the onset of a NTM have large uncertainties. As shown in figure 5(b'), the classical tearing stability term can be positive at the $q = 2$ surface for small island sizes. As it will be discussed in section 5 and previously discussed in the literature [24, 42], a non-perfect alignment of the EC deposition with the $q = 2$ resonant surface can even worsen the stability at small island sizes. Because toroidal effects are not taken into account in the solution of the MRE, including coupling between modes and the trigger from the $n = 1$ internal kink, the calculation of $\Delta'_{m,n}(w)$ has large uncertainties and this is a limitation common to all approaches based on the MRE. In the cases discussed here, where the MRE is used to evolve the island, uncertainties in the triggering condition tend to over-estimate the growth rate in the initial phase of evolution. Future implementations of the NTM module in TRANSP will address some of these limitations.

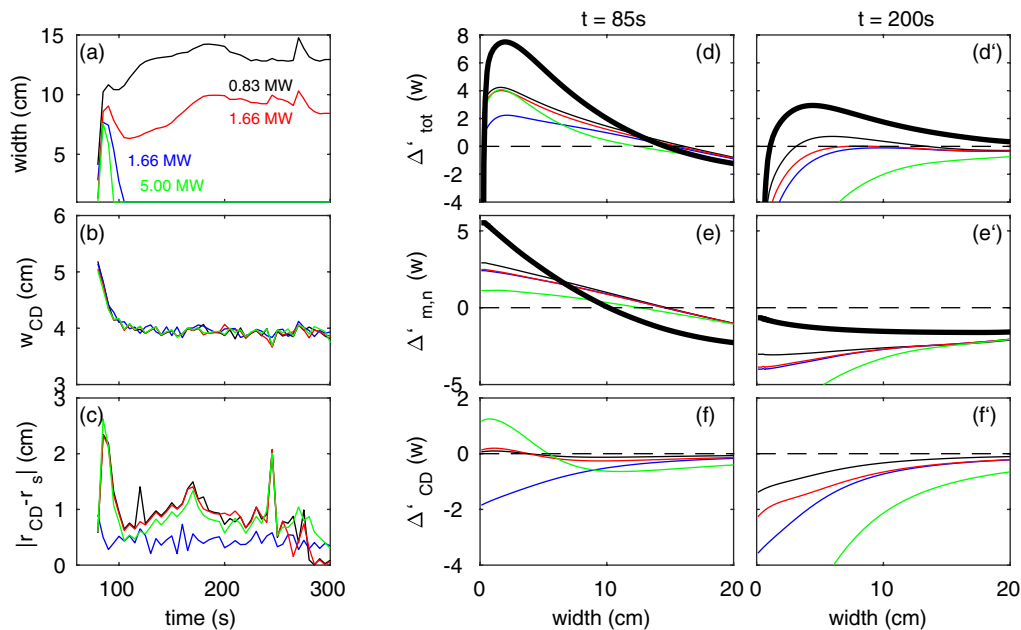


Figure 7. TRANSP/MRE simulations in the case of the (2, 1) mode for a scan of the input EC power. Left panel: (a) island width (b) ECCD deposition width, (c) distance between the EC deposition center and the rational surface. The blue and red curve use the same input EC power level, but the tolerance for alignment is more conservative in the blue case. Middle and right panels: (d) $\Delta'_{\text{tot}}(w)$, (e) $\Delta'_{m,n}(w)$, (f) $\Delta'_{\text{CD}}(w)$ for the same cases shown in the left panel, at two different time steps. The contributions to $\Delta'(w)$ for the unmitigated case are shown for comparison as thick black curves.

4.2. Simulation of pre-emptive NTM control and power requirements

Assuming that NTMs are metastable, i.e. that they can be triggered by a number of perturbations, including sawtooth crashes, ELMs, pellets, or magnetic fluctuations, and considering that the time scales of growth and locking of the (2, 1)-NTM are comparable to the time needed to switch EC power between transmission lines, it is argued that reserving the EC power for NTM control in the ITER baseline scenario is a better option than switching between applications.

The results are shown in figure 7. The tracking algorithm used here is based on ray-tracing calculations: for given magnetic equilibrium, density and temperature profiles at t_1 , the ray trajectories are calculated for poloidal angles in a range of 5 degrees around the mirror position at time t_1 , then an interpolation over the two values closest to the target rational surface is done to find the optimal poloidal angle. If the difference in radial location between the actual and the target radial deposition is smaller than the preset tolerance on the misalignment, dr_0 , then the poloidal angle is not adjusted, otherwise the needed corrections are applied. It is found in general that—except in the case of large sawtooth crashes, where the resonant surfaces undergo finite size shifts, this approach is very stable and it is well suited for the sensitivity studies carried out here. Other approaches will be considered in future implementations, which rely on checking the mirror position against the EC emission calculated by a synthetic diagnostic and that are therefore more realistic. The algorithm has been pre-programmed to allow for a maximum requested tolerance of $dr_0 = 0.5$ cm, which is very optimistic, but it provides a reference simulation that still offers a finite size deviation of the measured alignment $dr = |r_{\text{CD}} - r_s|$ with respect to a ‘perfect’

and unrealistic situation. We dub this case (blue curve) the ‘ideal’ alignment that is used for comparison with the other simulations. Only the (2, 1)-NTM is discussed here, since the (3, 2)-NTM is predicted to be stable with minimum applied power, if the ECCD is well aligned with the $q = 1.5$ surface. Similarly to what was found in the previous section, these simulations conclude that maintaining a good alignment with the rational surfaces is important, and that a large $|r_{\text{CD}} - r_s|$ at the onset on the NTM affects the time and the power needed for full suppression.

The blue and red curves assume the same input power of 1.66 MW, but they have different dr_0 . While the (2, 1)-NTM is fully suppressed shortly after the trigger in the case of ideal alignment (blue curve), it grows and saturates to about 10cm otherwise (red curve). Increasing the input power to 5 MW would suppress the mode in about 10s (green curve). In all cases, the (2,1)-NTM comes close to the threshold for locking within seconds after the onset. One may ask whether assuming a tolerance of 1 cm on the alignment of the EC with the resonant surface is an acceptable assumption or still technically challenging.

Because of the fast growth rate of the (2, 1)-NTM, the early stages of evolution of this mode might be particularly critical for stabilization and control, as shown in the central column, where the classical and ECCD contribution to the total $\Delta'_{\text{tot}}(w)$ are shown. The curves corresponding to the case without ECCD are shown for comparison (thick black). The deposition of ECCD close to the rational surface modifies the current profile and reduces the magnitude of $\Delta'_{m,n}(w)$ at all stages of evolution, by an amount that increases with the input power. However, this contribution is destabilizing at 85s for all the values of the island width. The $\Delta'_{\text{CD}}(w)$ is

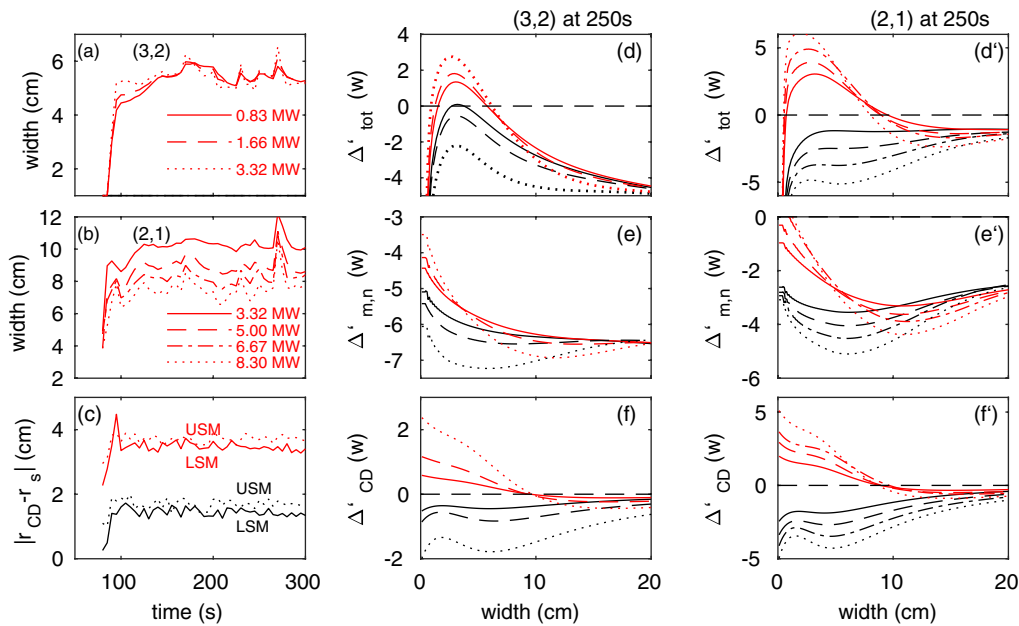


Figure 8. TRANSP/MRE simulations for higher pedestal pressure and late L–H transition with two values of dr_0 , tolerance on the alignment of the EC profile with the resonant surface, and for constant power on the $q = 1.5$ and $q = 2$ resonant surfaces. The USM is aiming at the $q = 1.5$ and the LSM at the $q = 2$ resonant surfaces. (a) (3,2)-NTM island width (b) (2,1)-NTM island width, (c) measured distance between the EC deposition center and the resonant surface r_s . The dotted lines refer to the USM, the solid lines refer to the LSM. Middle and right panels: ((d)–(d')) $\Delta'_{\text{tot}}(w)$, ((e)–(e')) $\Delta'_{m,n}(w)$, ((f)–(f')) $\Delta'_{\text{CD}}(w)$ for the (3,2) and the (2,1) mode, calculated at $t = 90$ s. TRANSP/GRE simulations in the case of the (2,1) mode for a scan of the input EC power. The red curves refer to the cases with larger dr_0 , the black curves to the cases with smaller dr_0 (all stable).

always stabilizing only in the case of ideal alignment (blue curve), but is destabilizing in all other cases, until the island width becomes comparable to w_{CD} . These cases correspond to a situation where the distribution of the EC current is unfavorable, being localized around the X-point of the magnetic island. When $w > w_{\text{CD}}$ the contribution of $\Delta'_{\text{CD}}(w)$ is always stabilizing because the EC drives the current inside the island. We also point out that the parametrization of the misalignment effect used here is valid only for $w \leq w_{\text{CD}}$ [24]. The plasma simulation with lower pedestal pressure is predicted to be stable against NTMs with pre-emptive application of the minimum available power for comparable values of the measured misalignment $dr \simeq 1$ cm and is not shown here.

5. Effect of misalignment on the stabilization and suppression

The effect of a loss of alignment between the EC deposition location and the rational surfaces where NTMs are triggered has been analyzed by other authors [10, 24, 42] who concluded that maintaining alignment within $0.5w_{\text{CD}}$ is a necessary requirement. Other studies came to more stringent conditions on the required alignment of less than 1 cm for a deposition width of 4–5 cm in order to suppress large NTMs [57, 58]. The time-dependent simulations discussed here are consistent with the former assessment, but they indicate that even a small loss of alignment at the NTM onset can affect the stabilization at later stages.

To complete the discussion started in the previous section, figures 8 and 9 show simulations where the maximum tolerance on the alignment is increased above 1 cm during the

entire flattop phase, for the two plasmas with higher and lower pedestal pressure respectively. It is assumed a constant level of input power on both rational surfaces, which—in the case of the plasma with higher pedestal pressure—is equal to one, two and four gyrotrons on the $q = 1.5$ surface, and four, six, eight and ten gyrotrons on the $q = 2.0$ surface.

The correction to $\Delta'_{\text{CD}}(w)$ due to a displacement of the maximum of the EC current density profile from the resonant radius is modeled using the parametrization from De Lazzari [24] and reported in equation (A.8) in the appendix. This term can be positive, thus destabilizing, if the EC is depositing on the X-point and its amplitude decreases from one to zero as the maximum of the EC current density profile (which peaks at r_{CD}) deviates from the resonant radius r_s . This term depends on the EC deposition width w_{CD} , on the island width and on the distance $|r_{\text{CD}} - r_s|$. Since the position of r_{CD} is calculated from a gaussian fit over the EC deposition profile, and the position of r_s is provided by TRANSP from spline interpolation of the q profile, the calculated $|r_{\text{CD}} - r_s|$ is subject to numerical errors and is not constant in time. Moreover, the rational surfaces evolve in response to the sawtooth cycle. Thus the poloidal angle of the UL is constant in time, but the actual measured $dr = |r_{\text{CD}} - r_s|$ can move around the target value. In both plasmas maintaining $dr \leq 2$ cm is a necessary condition for NTM suppression in both the high and low pedestal pressure cases (see figures 8 and 9). In the case of the (2,1)-NTM suppression is achieved with 3.32 MW in the plasma with higher pedestal pressure gradient and with 0.83 MW in the plasma with lower pedestal pressure (see figure 9). For larger values of dr the island grows rapidly to a width larger than w_{CD} independently on the amount of power

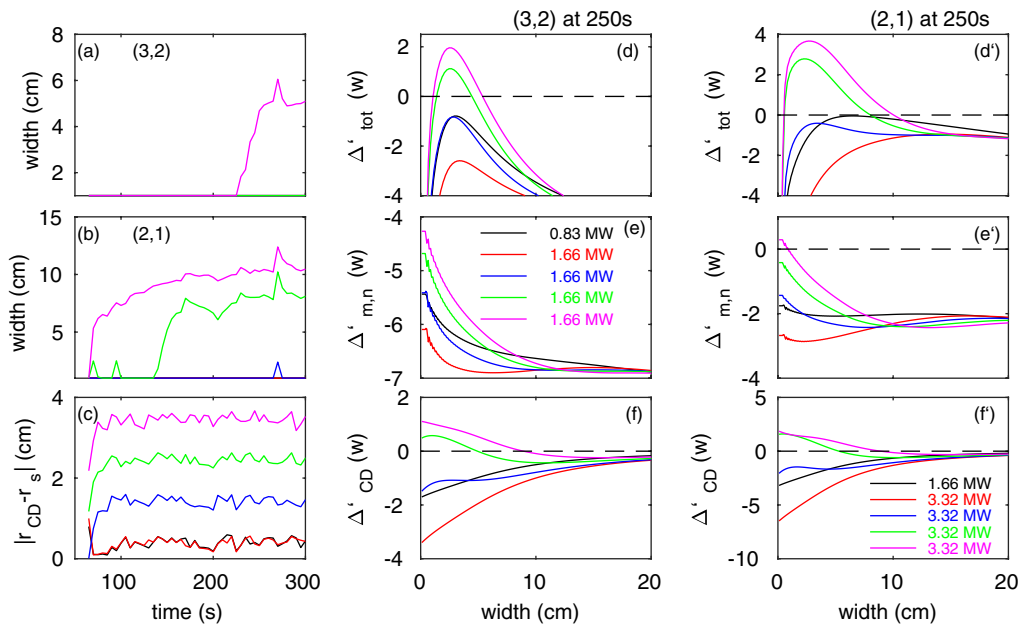


Figure 9. Same as figure 8, but for the case with lower pedestal pressure and earlier L–H transition. In this case only two values of power are assumed on both rational surfaces. The measured misalignment shown in (c) refers to the $q = 2$ surface, tracked with the LSM.

that is directed to the $q = 2$ surface. Increasing the injected power from 3.32 MW to 8.3 MW does provide only partial stabilization, by reducing the width of the saturated island by a factor of four from the unmitigated case, but it might be insufficient to avoid the locking of the (2, 1)-NTM.

In the case of the (3, 2)-NTM suppression is achieved with 0.83 MW of EC power in both high and low pedestal pressure, if $dr \leq 1$ cm. When the tolerance on the alignment is increased to 4 cm, the (3, 2)-NTM saturates at a size comparable to the unmitigated case even with higher EC power. Since the energy confinement reduction caused by an unmitigated (3, 2)-NTM with $w_{\text{sat}} = 7$ cm would be about 5%, but the reduction in Q for a mitigated NTM with 3.32 MW of injected power would be up to 10%, the decision whether to control this mode or not depends on the consequences that it has on the global stability of the plasma.

A difference between the cases with high and low pedestal pressure is that in the latter both the (3, 2)-NTM and the (2, 1)-NTM are triggered at later times by improving the alignment between the EC deposition and the rational surfaces. This is a consequence of the slower growth rate of the NTMs at onset in the low pedestal pressure plasma—as discussed in section 3—and it suggests that with adequate discharge design and control of the global plasma parameters the growth rate of NTMs can be reduced with advantages for NTM control. Because of the approach taken here and the consistent evolution of the magnetic equilibrium and the pressure profiles in response to a dynamical variation (magnitude and position) of the EC heating and current profiles, the values of power needed for full stabilization obtained are more optimistic than those found in previous analysis that included the effect of incorrect alignment of the EC on the NTM stability, but that was based on asymptotic results [24, 42]. Also, by tracking the resonant surface for pre-emptive control, the relaxation on the maximum misalignment are more optimistic than previous

estimates focussed on the stabilization of large magnetic islands [57, 58].

6. Effect of broadening of the deposition profile on stabilization

Excessive focussing of the LSM on the (2, 1) surface might be a problem, especially when the EC deposition is not aligned with the $q = 2$ surface, because it causes further destabilization of the island in its early stages of evolution, when its growth rate is largest. One might conclude that a broader deposition profile would reduce the destabilizing effect of a misalignment by enlarging the plasma region that falls in the shadow of the ECCD when the island is still small.

It should be noted that the simulations discussed here are assuming a single-beam, perfectly Gaussian deposition profile [25], while in reality the EC profile is the superposition of individual beams from distinct waveguides. This means that the modeled ideal focusing of the beam on the $q = 2.0$ surface, which was identified here as the main limitation for control, can be relaxed with appropriate pre-selection of the waveguides. In cases where the EC power is applied through the use of multiple waveguides a broader deposition profiles can be obtained by using waveguides connected to different upper launchers or different steering mirrors each pointing to a slightly different location. Another mechanism for broadening occurs naturally in the plasma, because of the presence of turbulence fluctuations that scatter the EC waves (see [59] and references therein). Waves are scattered in random directions and on average the beam axis will follow the original trajectory calculated in the absence of fluctuations. The average effect will be a broadening of the deposition profile and a consequent reduction of the maximum current drive peak, which has been deemed responsible for an increase of the requested power for stabilization [10]. This is not true if the

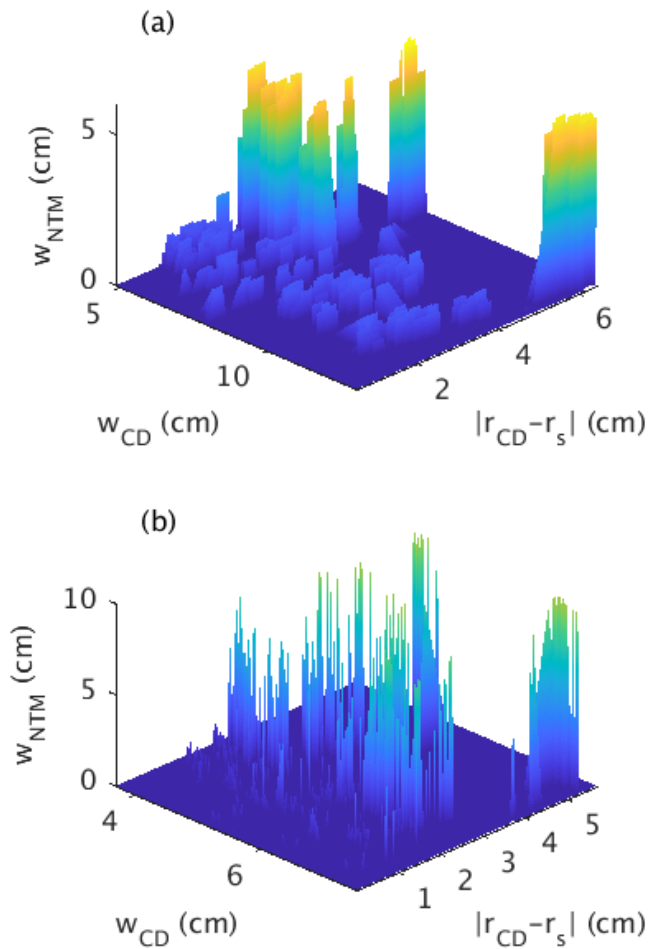


Figure 10. Histogram of the island width for different assumptions on the EC deposition width and of the measured alignment $|x_{CD} - x_j|$ for the (3, 2)-NTM (a) and for the (2, 1)-NTM (b).

beam propagation intersects the trajectory of a pellet or of a coherent structure in the scrape-off-layer. In this case the finite and localized perturbation in the density can scatter the beam from its original path, although this effect is not yet included in the TRANSP simulations.

The final deposition profile is the combination of the two effects, which are modeled here by increasing the initial beam waist. This correction to the initial launching conditions modifies w_{CD} at the resonance location; the corresponding value of $J_{CD,max}$ will be reduced according to the beam tracing calculations. As opposed to rescaling the magnitude of w_{CD} and $J_{CD,max}$ that enter directly in the $\Delta'_{CD}(w)$ contribution in equation (A.1), this approach accounts for the effect of the ECCD in modifying the temperature and current profile.

Figure 10 shows results from a set of simulations that scan the deposition width w_{CD} and the tolerance on the alignment dr_0 on the $q = 1.5$ and the $q = 2$ surface. The input power on the $q = 1.5$ surface is fixed and equal to 1.66 MW, while the power on the $q = 2$ surface is either 3.32 MW or 4.98 MW. The horizontal axes report the measured misalignment $dr = |r_{CD} - r_s|$ and the measured deposition width w_{CD} at the resonant surfaces.

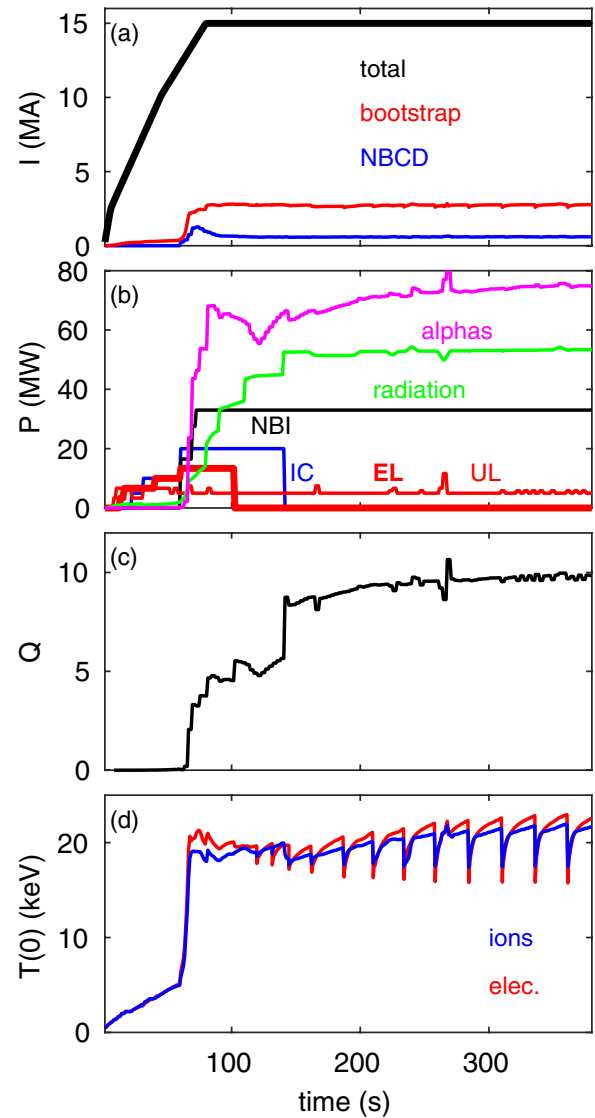


Figure 11. Simulation of the baseline scenario, with pre-emptive NTM control on the $q = 2$ surface. (a) plasma current and non-inductive contribution (b) heating power from fusion α s, external sources and impurity radiation (c) fusion gain (d) central temperature.

In both cases, the width of the island shrinks to zero only for $|r_{CD} - r_s|$ decreasing to zero. For increasing dr the width of the (3, 2)-NTM can be prevented from growing above a few centimeters only if the deposition profile is broadened. When broadening becomes too large the current drive efficiency is too low to have any effect on the island stability (for fixed input power). The results for the (2, 1)-NTM are qualitatively similar, although much more scattered. This is due mostly to the small value of the island at the onset. Also in this case, for fixed input power the size of the island can be prevented from growing only with a good alignment within 2 cm and for deposition width wider than approximately 5–6 cm.

The binned appearance of the data in the histogram is a consequence of having scanned the deposition width w_{CD} and the target alignment dr_0 over discrete values rather than having varied it continuously.

7. Conclusions and directions for future work

Modeling of NTM stabilization with EC and assessment of the power needed is one of the critical areas of the research in support of ITER. Calculations are commonly done using modified versions of the Rutherford equation and looking for solutions in the saturation limit, reviewed in [10]. The main difference between the analysis discussed here and previous assessment is that in this work the NTM stability is calculated by taking into account the plasma response to a simulated EC feedback control, by evolving the magnetic equilibrium, current and pressure profiles and the island width at the same time. Discussion of the rotation frequency of the island is not undertaken here, but focus is given to identify under which conditions the (2, 1)-NTM is prevented from growing above a few centimeters, typically 4–6 cm, to avoid locking. This approach highlights new aspects important for NTM control on ITER and different from typical situations observed in present-day experiments, although many uncertainties still remain due to the approximations intrinsic in the reduced models that are used.

First, the large neoclassical drive and β_N on ITER make NTMs metastable and susceptible of being triggered by any external or internal perturbation [27]; thus, suppressed NTMs can be triggered soon after the EC power is removed from the respective rational surfaces. These results should be verified by more advanced calculations that include toroidal effects in the calculation of the tearing stability term $\Delta'_{m,n}(w)$ and that evolve both the magnetic island and its rotation frequency over the MHD and transport time scales. This can possibly be done only using nonlinear 3D MHD codes coupled to ray-tracing calculations.

Within the limits of the approximations used here, the time-dependent simulations indicate that maintaining a constant level of power on the $q = 2$ rational surface, rather than actively searching for a mode that has grown above a detection threshold is more favorable to the stabilization and suppression of the (2, 1)-NTM.

Second, alignment of the EC deposition location with the resonant surfaces is critical. This is no surprise and it has been stressed by other authors [10, 24, 42, 57, 58]. Alignment depends on diagnostics, on the accuracy of the magnetic equilibrium reconstruction, on the accuracy of the EC system alignment itself and on defocussing effects from turbulence. Similar to previous analysis [42], we also find that a distance comparable to approximately half the EC deposition width is the maximum deviation from an ideal alignment that is tolerated for the success of NTM control. A lower limit of 2 cm is obtained assuming a perfectly focussed beam, but this limit might be relaxed due to scattering effects and to artificially broadening via selection of the injection waveguides.

When the effect of uncertainty in the alignment of the ECCD is taken into account, an upper limit for the stabilization of the (2, 1) of 5 MW when $dr \simeq 2$ cm is found, provided the $q = 2$ is constantly tracked. Figure 11 shows a simulation that puts together everything learnt from the simulations discussed in this work. Here it is assumed that the LSM is tracking the $q = 2$ as soon as the plasma enters H-mode, that

the combined effect of using multiple waveguides and turbulence broadens the EC deposition width up to about 7 cm and that the EC power is reserved to the UL in the flattop. The EC power is used in the ramp-up for H-mode access, with up to 20 MW, combining the equatorial and the upper launcher. The upper launcher starts tracking the $q = 2$ surface at the entry to H-mode with constant 5 MW of power for pre-emptive control. At 100s the power on the equatorial launcher is redirected to the upper launcher and reserved for NTM control. The reserved gyrotrons are promptly turned-on when the diagnostics detect an island (i.e. when the width calculated by the MRE satisfies $w > w_{ECE} = 4$ cm), as indicated by the occasional spikes in the EC waveform. This simulation achieves $Q = 10$, but it does so only by turning-off the IC power in the flattop.

Approaches based on MRE are intrinsically affected by large uncertainties due to the use of approximation in the calculation of a threshold on the onset of the NTM, the neglect of toroidal effects in the calculation of the tearing stability, among the others. These simulations have highlighted a need for early stabilization, but they have also identified areas where a more integrated approach is needed to resolve uncertainties due to a too frequent triggering of the (2, 1)-NTM. This includes (a) evolving the coupled equations of the island width and rotation over transport time scales and (b) include the effect of the presence of a finite island on local flattening of the density and temperature profiles, (c) include toroidal effects in the calculation of the tearing stability term, which might affect significantly the instability threshold. An improved reduced model could then be used to assess the ITER plasma response to techniques presently used for NTM control, like sweeping the EC deposition across the resonant surface, which has not been assessed here.

Research on NTM stabilization and development of complex control algorithms is very active and highly successful on present-day experiments and extrapolation of these techniques to ITER is critical for designing robust control algorithms. The use of time-dependent simulations that combine the plasma evolution with simulated schemes for feedback control can represent in this regard a valuable tool for design of robust control algorithms on ITER, by testing these schemes with hardware constraints and high fidelity physics models.

Acknowledgments

We thank O. Sauter, S. Nowak and the colleagues at PPPL, F4E and IO who have contributed to the development of this work with suggestions and feedback. This work is supported by ITER contract IO/RFQ/13/9550/JTR and by DOE contract DEAC02-09CH11466. The views and opinions expressed herein do not necessarily reflect those of the ITER Organization. This manuscript is based upon work supported by the U.S. Department of Energy, Office of Science, Office of Fusion Energy Sciences, and has been authored by Princeton University under Contract Number DE-AC02-09CH11466 with the U.S. Department of Energy. The publisher, by accepting the article for publication acknowledges, that the

United States Government retains a non-exclusive, paid-up, irrevocable, world-wide license to publish or reproduce the published form of this manuscript, or allow others to do so, for United States Government purposes.

Appendix

The equations for the evolution of the island width w interfaced with TRANSP are based on the work by Fredrickson [17], to which two terms for the ECCD and for the ECH have been added:

$$\frac{dw}{dt} = 1.22 \frac{\eta}{\mu_0} [\Delta'_{m,n}(w) + \Delta'_{\text{NC}}(w) + \Delta'_{\text{pol}}(w) + \Delta'_{\text{GGJ}}(w) + \Delta'_{\text{CD}}(w)] \quad (\text{A.1})$$

where μ_0 the magnetic permeability and η the neoclassical plasma resistivity, which is calculated in TRANSP using the NCLASS libraries [60]. For $\eta = 6.8 \times 10^{-7} \Omega \text{ cm}$ at the $q = 1.5$ resonant surface and $\eta = 1.78 \times 10^{-6} \Omega \text{ cm}$ at the $q = 2$ resonant surface, the corresponding resistive time scales for the growth of the island are $\tau_R = 284 \text{ s}$ and $\tau_R = 228 \text{ s}$.

The terms on the right hand side are summarized below. For an extensive description of how they have been derived the reader is referred to the original references. The $\Delta'_{m,n}(w)$ represents the drive or damping on the tearing mode imposed by the external solution. In TRANSP a quasi-cylindrical approximation is made, so that the $J_0(r)$ and $q(r)$ are not related by the simple cylindrical approximation, but they are integrated from the toroidal magnetic equilibrium code [17]. This approach gets the rational surfaces in the right location and maintains the equilibrium current $J_0(r)$ and the derivative $J'_0(r)$ terms consistent [17].

The second term on the right hand side represents the destabilizing effect of the bootstrap current J_{BS} and is given by [35]:

$$\Delta'_{\text{NC}}(w) = k_1 \frac{16J_{\text{BS}}}{s \langle J \rangle} \frac{w}{w^2 + w_d^2} \quad (\text{A.2})$$

where

$$w_d = 5.1k_d \frac{r_s}{\sqrt{\epsilon sn}} \left(\frac{\chi_{\perp}}{\chi_{\parallel}} \right)^{1/4} \quad (\text{A.3})$$

measures the extent to which the cross-field transport can support a parallel temperature or density gradient [35]. Here s is the magnetic shear, r_s the radius of the rational surface, ϵ the local aspect ratio and k_1 and k_d two calibration coefficients. The correction to the w^{-1} dependence accounts for the existence of a threshold for instability of the tearing modes. The coefficient k_1 accounts for the fact that the derivation of the neoclassical term is not exact.

The third term on the right hand side is the polarization term [36]:

$$\Delta'_{\text{pol}}(w) = -k_2 \frac{\rho_{\theta i}^2 \beta_{\text{pol}} g}{w^3} \left(\frac{L_q}{L_p} \right)^2 \quad (\text{A.4})$$

Here $L_{q,p}$ represent the local gradient scale length of the q and pressure profile respectively, β_{pol} is the plasma poloidal beta,

$\rho_{\theta i}$ the ion poloidal gyroradius and the parameter $g \simeq \epsilon^{3/2}$ and it approaches unity in the limit of low collisionality [17]. The polarization term is important for small island sizes and it becomes a small contribution in the case of large island sizes.

The fourth term on the right hand side is the Glasser-Green-Johnson term [61]:

$$\Delta'_{\text{GGJ}}(w) \approx -5.4k_4 \frac{\beta_{\text{pol}} \epsilon^2 L_q^2 q^2 - 1}{r_s w |L_p| q^2} \quad (\text{A.5})$$

The form used here is the derivation by Houlberg [60].

Finally, the last term is the stabilizing contribution of the localized EC current drive. There are several expressions for this term. The one used here is from Bertelli *et al* in the limit of no EC power modulation [23]:

$$\Delta'_{\text{CD}}(w) = k_6 16\pi^{1/2} \frac{\mu_0 L_q}{B_p} \frac{J_{\text{CD,max}}}{w_{\text{CD}}} F(\tilde{w}) G(\tilde{w}, x_{\text{dep}}) \quad (\text{A.6})$$

with [23]

$$F(\tilde{w}) = 0.25 \frac{1 + 0.96\tilde{w}}{1 + \tilde{w}(1.5 + \tilde{w}(0.43 + 0.64\tilde{w}))} \quad (\text{A.7})$$

where $\tilde{w} = w/w_{\text{CD}}$ is the island width normalized to the EC deposition width. The function $F(\tilde{w})$ attains its maximum value of 0.25 in the limit of $\tilde{w} = 0$ and decays asymptotically as $(3/8)\tilde{w}^2$ in the limit of large \tilde{w} , showing how the effective stabilization is reduced as the island width exceeds the EC deposition width w_{CD} . The term $G(w)$ represents the effect of misalignment of the EC deposition with the resonant surface. This term is important for the studies presented herein. The expression used in TRANSP uses the derivation in De Lazzari *et al* [24]:

$$G(\tilde{w}, x_{\text{dep}}) = 1 - 2 \frac{x_{\text{dep}}}{g(\tilde{w})} e^{-\left(\frac{x_{\text{dep}}}{g(\tilde{w})}\right)^2} \int_0^{x_{\text{dep}}/g(\tilde{w})} dt e^{t^2} \quad (\text{A.8})$$

with

$$g(\tilde{w}) = \frac{0.38\tilde{w}^2 + 0.26\tilde{w} + 0.5}{\tilde{w} + 1} \quad (\text{A.9})$$

where $x_{\text{dep}} = (r_{\text{dep}} - r_s)/w_{\text{dep}}$ represents the deposition location relative to the resonant radius, normalized to the EC deposition width. We note that there is a typo in equation (15) of [24], although the figures in that paper have been derived using the correct formulation. This term is important for the studies undertaken herein, which aim at assessing the effects of systematic misalignments or the effect of transient misalignments, like those caused by a sawtooth crash.

ORCID iDs

F.M. Poli  <https://orcid.org/0000-0003-3959-4371>

References

- [1] Henderson M.A. *et al* 2015 *Phys. Plasmas* **22** 021808
- [2] Farina D., Henderson M.A., Figini L. and Saibene G. 2014 *Phys. Plasmas* **21** 061504
- [3] Farina D., Henderson M.A., Figini L., Ramponi G. and Saibene G. 2012 *Nucl. Fusion* **52** 033005

- [4] Henderson M.A. et al 2008 *Fusion Sci. Technol.* **53** 139
- [5] Ramponi G., Farina D., Henderson M.A., Poli E., Saibene G. and Zohm H. 2007 *Fusion Sci. Technol.* **52** 193
- [6] Zohm H. et al 2007 *Plasma Phys. Control. Fusion* **49** B341
- [7] Reiman A.H. 1983 *Phys. Fluids* **26** 1338
- [8] Maraschek M. 2012 *Nucl. Fusion* **52** 074007
- [9] Hegna C. and Callen J. 1997 *Phys. Plasmas* **4** 2940
- [10] Poli E. et al 2015 *Nucl. Fusion* **55** 013023
- [11] Hawryluk R. 1981 An empirical approach to tokamak transport *Physics of Plasmas Close to Thermonuclear Conditions: Proc. of the Course Held in (Varenna, Italy, 27 August–8 September 1979) vol 1*, ed B. Coppi (Elsevier) p 1946 (<http://w3.pppl.gov/transp>)
- [12] Rutherford P.H. 1973 *Phys. Fluids* **16** 1903
- [13] Wehner W. and Schuster E. 2012 *Nucl. Fusion* **52** 074003
- [14] Boyer M. et al 2015 *Nucl. Fusion* **55** 053033
- [15] Boyer M. et al 2017 *Nucl. Fusion* **57** 066017
- [16] Goumiri I. et al 2016 *Nucl. Fusion* **56** 036023
- [17] Fredrickson E., Bell M., Budny R.V. and Synakowski E. 2000 *Phys. Plasmas* **7** 4112
- [18] Chang Z. et al 1998 *Phys. Plasmas* **5** 1076
- [19] White R.B., Monticello D.A., Rosenbluth M.N. and Waddell B.V. 1977 *Phys. Fluids* **20** 800
- [20] Westerhof E., de Blank H.J. and Pratt J. 2016 *Nucl. Fusion* **56** 036016
- [21] Fredrickson E.D., McGuire K.M., Goldston R.J., Bell M.G., Grek B., Johnson D.W., Morris A.W., Stauffer F.J., Taylor G. and Zarnstorff M.C. 1987 *Nucl. Fusion* **27** 1897
- [22] Fredrickson E.D. 2002 *Phys. Plasmas* **9** 548
- [23] Bertelli N., De Lazzari D. and Westerhof E. 2011 *Nucl. Fusion* **51** 103007
- [24] De Lazzari D. et al 2009 *Nucl. Fusion* **49** 075002
- [25] Poli E. et al 2001 *Comput. Phys. Commun.* **136** 90
- [26] Fevrier O., MAget P., Lutjens H. and Beyer P. 2017 *Plasma Phys. Control. Fusion* **59** 044002
- [27] Sauter O. et al 2010 *Plasma Phys. Control. Fusion* **52** 025002
- [28] Waltz R.E. et al 1997 *Phys. Plasmas* **4** 2481
- [29] Kinsey J.E. et al 2003 *Fusion Sci. Technol.* **44** 763
- [30] Porcelli F., Boucher D. and Rosenbluth M.N. 1996 *Plasma Phys. Control. Fusion* **38** 2163
- [31] Snyder P.B. et al 2011 *Nucl. Fusion* **51** 103016
- [32] Troyon F. et al 1984 *Plasma Phys. Control. Fusion* **26** 209
- [33] Martin Y.R. et al 2008 *J. Phys.: Conf. Ser.* **123** 012033
- [34] Sauter O. et al 1997 *Phys. Plasma* **4** 1654
- [35] Fitzpatrick 1995 *Phys. Plasmas* **2** 825
- [36] Wilson H. et al 1996 *Phys. Plasmas* **3** 248
- [37] Chang Z. et al 1995 *Phys. Rev. Lett.* **74** 4663
- [38] Udintsev V.S. et al 2012 *Proc. 24th Int. Conf. on Fusion Energy (San Diego, 2012)* [ITR/P5-41] (www-naweb.iaea.org/napc/physics/FEC/FEC2012/index.htm)
- [39] Snipes J.A. et al 1900 *Fusion Eng. Des.* **87** 1900
- [40] La Haye R.J. et al 2006 *Nucl. Fusion* **46** 451
- [41] Chang Z. and Callen J.D. 1990 *Nucl. Fusion* **2** 219
- [42] La Haye R.J. et al 2008 *Nucl. Fusion* **48** 054004
- [43] La Haye R.J. et al 2017 *Nucl. Fusion* **57** 014004
- [44] Kolemen E. et al 2013 *Fusion Eng. Des.* **88** 2757
- [45] Kolemen E. et al 2014 *Nucl. Fusion* **54** 073020
- [46] Welander A.S. et al 2015 *Proc. of the IEEE 26th Symp. on Fusion Engineering* pp 1–5
- [47] Felici F. et al 2012 *EPJ Web Conf.* **32** 02005
- [48] Felici F. et al 2013 *Nucl. Fusion* **53** 113018
- [49] Canal G.P. et al 2013 *Nucl. Fusion* **53** 113026
- [50] Kim D. et al 2014 *Phys. Plasmas* **21** 061503
- [51] Rapson C. et al 2014 *Fusion Eng. Des.* **89** 568
- [52] Stober J. 2015 *EPJ Web Conf.* **87** 02017
- [53] Poli E. et al 2010 *Plasma Phys. Control. Fusion* **52** 12402
- [54] Ishizawa A. and Nakajima N. 2010 *Phys. Plasmas* **17** 072308
- [55] Muraglia M. et al 2011 *Phys. Rev. Lett.* **107** 095003
- [56] Hornsby W.A. et al 2015 *Plasma Phys. Control. Fusion* **57** 54018
- [57] Urso L., Zohm H., Isayama A., Maraschek M., Poli E., ASDEX Upgrade Team and JT-60U Team 2010 *Nucl. Fusion* **50** 025010
- [58] van den Brand H., de Baar M.R., Lopes Cardozo N.J. and Westerhof E. 2012 *Plasma Phys. Control. Fusion* **54** 094003
- [59] Weber H., Maj O. and Poli E. 2015 *EPJ Web Conf.* **87** 01002
- [60] Houlberg W.A. et al 1997 *Phys. Plasmas* **4** 3230
- [61] Gorelenkov N. et al 1996 *Phys. Plasmas* **3** 3379